Journal of Environmental Management 304 (2022) 114262

Contents lists available at ScienceDirect

Journal of Environmental Management

journal homepage: www.elsevier.com/locate/jenvman

Seagrass restoration monitoring and shallow-water benthic habitat mapping through a photogrammetry-based protocol

Daniele Ventura [a,*], Gianluca Mancini [a], Edoardo Casoli [a], Daniela Silvia Pace [a], Giovanna Jona Lasinio [b], Andrea Belluscio [a], Giandomenico Ardizzone [a]

[a] Department of Environmental Biology and Ecology, University of Rome 'La Sapienza', V. le dell'Università 32, 00185, Rome, Italy
[b] Department of Statistics Sciences, University of Rome 'La Sapienza', V. le dell'Università 32, 00185, Rome, Italy

ARTICLE INFO

Keywords:
Structure-from-Motion (SfM)
Posidonia oceanica
3D points clouds
Restoration ecology
Remote sensing

ABSTRACT

Seagrasses rank among the most productive yet highly threatened ecosystems on Earth. Loss of seagrass habitat because of anthropogenic disturbances and evidence of their limited resilience have provided the impetus for investigating and monitoring habitat restoration through transplantation programmes. Although Structure from Motion (SfM) photogrammetry is becoming a more and more relevant technique for mapping underwater environments, no standardised methods currently exist to provide 3-dimensional high spatial resolution and accuracy cartographic products for monitoring seagrass transplantation areas. By synthesizing various remote sensing applications, we provide an underwater SfM-based protocol for monitoring large seagrass restoration areas. The data obtained from consumer-grade red-green-blue (RGB) imagery allowed the fine characterization of the seabed by using 3D dense point clouds and raster layers, including orthophoto mosaics and Digital Surface Models (DSM).

The integration of high spatial resolution underwater imagery with object-based image classification (OBIA) technique provided a new tool to count transplanted *Posidonia oceanica* fragments and estimate the bottom coverage expressed as a percentage of seabed covered by such fragments. Finally, the resulting digital maps were integrated into Geographic Information Systems (GIS) to run topographic change detection analysis and evaluate the mean height of transplanted fragments and detect fine-scale changes in seabed vector ruggedness measure (VRM). Our study provides a guide for creating large-scale, replicable and ready-to-use products for a broad range of applications aimed at standardizing monitoring protocols in future seagrass restoration actions.

1. Introduction

Seagrasses are considered one of the most important shallow-marine ecosystems in terms of goods and services for their ecological, physical, economic, and bio-indicator roles (Duarte, 2002; Larkum et al., 2006). Some seagrass species can form extensive meadows that can provide key ecosystem services, including erosion control (Ondiviela et al., 2014), carbon sink (Duarte et al., 2010) other than serving as a provision of food for herbivorous fauna (Klumpp and Nichols, 1983) and nursery grounds for many marine species (Seytre and Francour, 2014), supporting fish, shellfish, and invertebrate assemblages (Heck et al., 2003).

Unfortunately, since the last century, seagrass meadows are rapidly declining due to both natural processes (Boudouresque et al., 2009) and human-mediated impacts such as boat anchoring (Francour et al., 1999), alien species introduction (Casoli et al., 2021; Telesca et al., 2015), and fish farming (Delgado et al., 1999). Continual loss of seagrasses coupled with the decline of coastal environmental quality has resulted in national and international legislation and policies for the protection and conservation of seagrass habitat (Unsworth et al., 2019). For example, they are protected globally by the Convention of Biological Diversity (1992) and locally by national laws and acts such as the Wildlife and Countryside Act (1981) in England, the Water Framework Directive (2000) in Europe, the Biological diversity Act (2002) in India, the Chesapeake Bay Program (1983) in the United States and the Great Barrier Reef Water Quality Protection Plan (2005) in Australia. Nevertheless the robust legal framework, most seagrass meadows remain under significant pressure resulting in a decline condition (Unsworth et al., 2019). For this reason, several guidelines were developed focused on mitigation measures to prevent further losses and facilitate recovery through restoration actions (Cunha et al., 2012).

* Corresponding author.
E-mail address: daniele.ventura@uniroma1.it (D. Ventura).

https://doi.org/10.1016/j.jenvman.2021.114262
Received 24 June 2021; Received in revised form 29 November 2021; Accepted 6 December 2021

Although both seagrass experimental trials and large-scale transplanting operations have been carried out (Van Katwijk et al., 2009), little effort has yet been made to define new methods to remotely follow over time the survival and growth of the transplanted fragments over large areas, without direct manipulation of plants. The current methods to monitor these operations rely on self-contained underwater breathing apparatus (SCUBA) divers using direct in-situ measures, implying manipulation of fragments and leaves, especially during shoot density counts. Even if shoot density remains a key measure for evaluating the health condition of meadow, however, the success of transplanting operations can be also assessed by using other metrics such as the seagrass percent cover compared to the unvegetated sea bottom (Rezek et al., 2019), the survival of the transplant, and the rhizome expansion/elongation (Asriani et al., 2018; Paling et al., 2001). Traditional underwater counts can provide useful data for ecological studies but there is the potential for observer bias (Inglis and Smith, 1995), non-repeatability, inaccurate underwater positioning, damage and stress for the transplanted vegetal material (especially if monitoring is carried out by non-marine scientist diver). Moreover, *in situ* counts methods techniques are labour-intensive and time-consuming for underwater operators, implying safety, monitoring and management constraints during periodic inspection of restoration activities, especially for large scale transplanted areas.

Modern technological advances in computer vision have led to increased use of new powerful systems for processing imagery to create 3D surfaces of physical structures digitally, allowing these traditional methods to be substantially improved upon (Nex and Remondino, 2014). Structure from Motion (SfM) photogrammetry provides new opportunities to extract a plethora of fine-scale variables from 3D digital models of the underwater environment (Abadie et al., 2018; Marre et al., 2020), directly derived from overlapping two-dimensional camera images taken from different points of view. SfM-derived 3D point clouds, triangular meshes, and orthomosaics can be analysed in several ways, providing an excellent tool for accurate measurement of lengths, areas, and volumes that are difficult or even impossible to get *in situ* with traditional methods (Bayley et al., 2019). Even if such products have a key role in assessing 3D habitat complexity and health conditions of specific biotopes such as biogenic reef (Burns et al., 2019; Ventura et al., 2020) they can provide also valuable information for fine-scale assessment and monitoring of seagrass limits and their level of fragmentation (Marre et al., 2020; Rende et al., 2020).

Here we propose a novel and transferable SfM-based protocol for monitoring seagrass transplantation sites, aiming to define the main steps needed to create centimetre-level accuracy cartographic products and large-scale 3D models. Our work aims to synthesize various geoprocessing routines into a single workflow to remotely measure specific seagrass metrics to follow over time both the survival and growth of the transplanted fragments and the effects of transplanting operations on the impacted site. Because this method can be easily transferred to other seagrass restoration programmes outside the Mediterranean basin, we hope our protocol will provide a baseline design to standardise the applications of photogrammetry in the field of seagrass restoration and monitoring, by summarising a range of approaches already in use in the most diverse fields of spatial ecology, remote sensing and seabed habitat mapping.

2. Material and methods

2.1. Model species and study site

Posidonia oceanica (L.) Delile, 1813 is the most widespread and important endemic seagrass species in the Mediterranean Sea. *P. oceanica* forms topographically complex habitats thriving either on sandy or rocky bottoms. The entanglement of the horizontal and vertical rhizomes together with the radical system leads to a tridimensional biogenic structure called "*matte*", which retains the fine sediments trapped by leaf canopy (Larkum et al., 2006). Loss of *Posidonia* meadows across the globe in human-dominated coastal marine ecosystems, coupled with evidence of their slow regeneration and resilience times, have provided the impetus for investigating the restoration of such habitats (Bastyan and Cambridge, 2008). Because the natural recovery of impacted *Posidonia* meadows may require decades to centuries, restoration actions based on the removal of physical stressors followed by active transplantation of new plants could be an integral part of both protection and conservation strategies. In the last decade, *Posidonia* restoration actions have become gradually more popular both using donor meadows (Verduin et al., 2012) or naturally detached fragments (Balestri et al., 2011).

2.2. Timing of transplant activities and SfM surveys

Fieldworks were carried out on the east side of Giglio Island (central Tyrrhenian Sea, Italy), inside one of the four restoration sites located into the shipyard areas identified after the Costa Concordia shipwrecking (Fig. 1). After the Costa Concordia disaster (January 2012), the area (~500 m^2 extending from 10 to 19 m depth) was exposed to multiple disturbance events due to both the physical presence of the wreck and removal activities, which affected the natural *P. oceanica* meadow, leading to its regression and leaving on the seabed a bare substratum consisting of dead *matte* (Mancini et al., 2019; Toniolo et al., 2018). At the end of the wreck removal operations (July 2014) and after the seabed cleaning phase (April 2018), the natural environmental conditions were restored, ensuring the suitability of the area for transplant operations (Toniolo et al., 2018). Indeed, in 2019 transplanting operation has begun inside the shipyard area by using iron stakes to install into the dead *matte* bed detached fragments of *P. oceanica* collected around the coastal area of the Island (naturally generated from the meadow as a consequence of storms or anthropogenically derived by boat anchoring). Before starting the transplant activities in the study area, the first SfM photogrammetric survey was carried out in May 2020 to produce the first point cloud data of the site. At the end of September 2020, the same area was mapped again to generate the second point cloud data to be used for image and change detection analyses.

2.3. Field preparation before image acquisition

Before starting the transplantation, the area was divided into smaller areas (N = 20) by a 5 × 5 m grid defined by metal stakes and ropes. To ensure ropes' visibility in the acquired imagery, they have been cleaned periodically to prevent fouling events. This framing was used to sectorise the seabed to work with smaller areas and speed up further data processing. Moreover, 13 fixed monitoring quadrats (1 × 1 m) have been randomly installed for fine-scale measurements and accuracy assessments.

2.4. Above water estimation of reference markers coordinates

Because accurate positioning and data georeferencing are key aspects for mapping and monitoring many ecological processes relying on Geographic Information Systems (GIS) based on SfM applications, we deployed 15 reflective white targets (30 × 30 cm) to be used as reference markers or Ground Control Points (GCPs) inside the area to ensure both global and internal accuracy across datasets (Fig. 2a). The use of GCPs improved SfM products geolocation with respect to real-world coordinates and ensured accurate measurements of geometries within the end-products (Kalacska et al., 2020). GCPs was installed on some vertices of the grid and inside the 5 × 5 m quadrats by using iron stakes.

Considering that in the proximity of our working area no triangulation station, also known as a trig point, are available, we estimated the absolute coordinates of an unknown point along the coastline to be used later to place the base Global Navigation Satellite System (GNSS) unit, ensuring a very short baseline during the RTK survey for GCPs

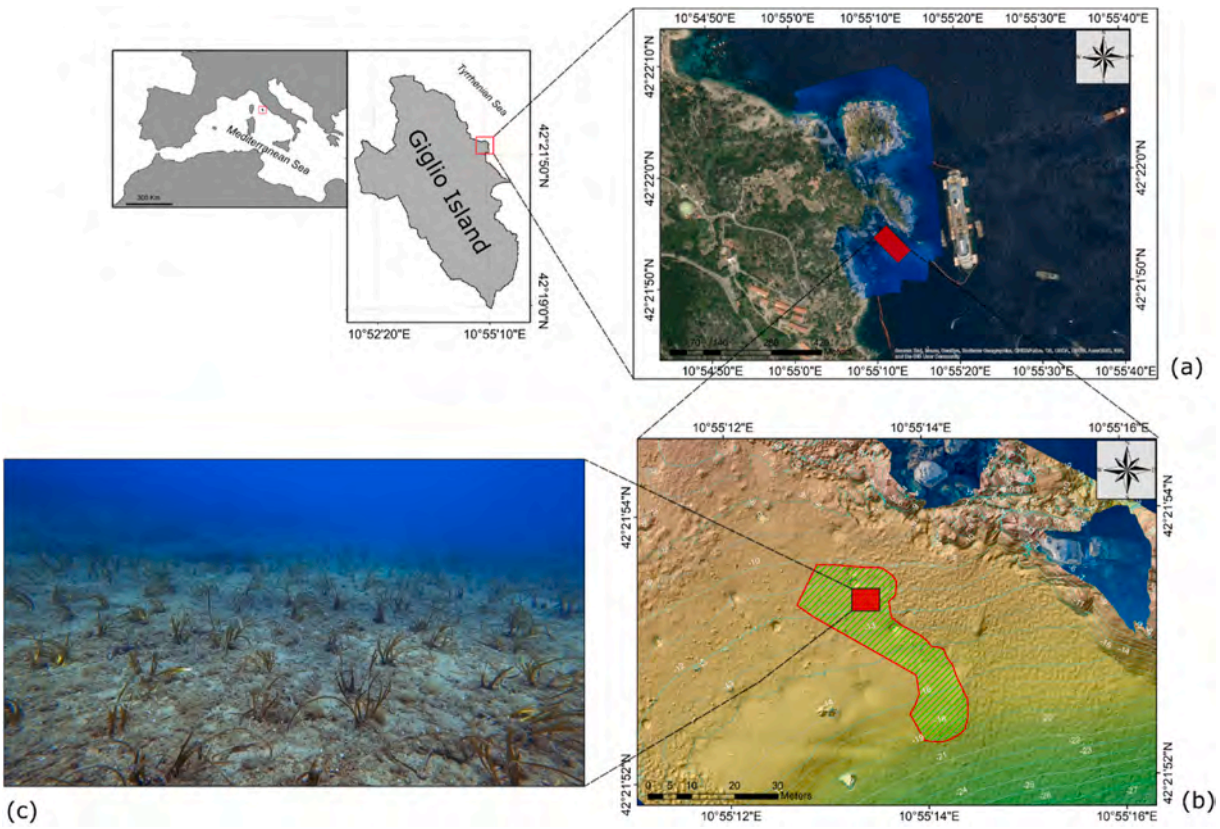

Fig. 1. The study site of Giglio Island used to develop our procedural protocol aimed at monitoring transplantation intervention on seagrass species. (a) Transplanting operations started in 2019, were focused on the restoration of *Posidonia oceanica* meadow impacted by the shipwrecking of the Costa Concordia cruiser. (b) the highlighted area by the red polygon is one of the four transplanting sites with a spatial extension of ~500 m^2, where in summer 2020, we applied our protocol (c) Underwater view of the transplanting area with transplanted *Posidonia* fragments planted into the dead *matte* and sandy substrata by iron stakes. (For interpretation of the references to color in this figure legend, the reader is referred to the Web version of this article.)

acquisition. For this task, raw GNSS coordinates (in U-Blox format) have been recorded for 8 h by a static survey with Emlid Reach RS+ (https://emlid.com/reachrs/), a low-cost single-frequency (L1 - 1575.42 MHz) GNSS receiver. The open-source software package RTKLib (Takasu and Yasuda, 2009) was used for computing Post-Processed Kinematics (PPK) corrections (see appendix A in supplementary material for more details on GNSS survey and PPK/RTK procedures). Subsequently, coordinates of GCPs were determined from the surface by using another Emlid Reach RS + unit (rover), configured in RTK mode and mounted on a rigid marker buoy. The buoy was moved from the surface on every GCP by a snorkelling operator (Fig. 2a). The buoy's perpendicular position over GCPs was ensured by a plumb bob (400 g) visually liking the phase centre of the antenna to the seabed. On the plumb bob, a digital level gauge (Onset Computer Company #U20_001–02, http://www.onsetcomp.com/products/data-loggers/u20-001-02), with a resolution of 4.1 mm and an accuracy of ±15 mm, was mounted to measure water depth (i.e. the -Z-axis of each GCP). The ReachView 3 app (https://emlid.com/the-new-reachview-3-simplifies-rtk-data-collection/available for Android and iOS mobile devices) was used to set up the RTK parameters and to collect GCPs. Each GCP was surveyed with the rover unit for approximately 1 min to ensure an accurate measurement. Even if this operation was carried out from the surface, the mobile device used should be protected by a waterproof case to prevent any damage. In our case, GCPs were measured in the European Terrestrial Reference System 1989 (ETRF 89) and projected to the Universal Transverse Mercator (UTM 32N), but more than a thousand coordinate systems are available in the app.

2.5. Underwater image collection method for SfM processing

Due to the extent of the working area to overcome the limitations linked to traditional SCUBA diving, a diver propulsion vehicle (DPV, Suex X-joy 7) was used to optimise image acquisition (Fig. 2b). The DPV was equipped with a spirit level, compass, and depth gauge to help the diver keep his path as constant as possible during photo acquisition. Below the DPV, a GoPro Hero 5 Black action camera (1/2.3″ CMOS rolling shutter; 1.53 μm pixel spacing; 4000 × 3000 pixel captured image size; 2.68 mm nominal focal length) was installed using an adhesive mount with an adjustable arm. Still images (12 MP) were acquired pointing the camera down towards the substrate at a near-nadir position, 4 m above the seabed, ensuring a subcentimeter Ground Sample Distance or GSD (i.e. the distance between the centre of two pixels measured on the seafloor) useful for micro-scale assessments. Considering that the DPV speed was set to 'low' (~25 m/min) and the wide-angle of the camera (Diagonal FOV 133.6° at 16:9), to collect regularly spaced images with an in-track overlap of 80%, photos were acquired every 5 s with the built-in time-lapse function. Since at least 65% cross-track overlap was required to ensure good model generation, the transects were spaced no more than 4 m. Due to non-optimal light conditions (cloud cover) raw (.GPR) format which took full advantage of the image sensor's capabilities were used. After DNG conversion, GPR files were opened in the free photo-editing software RawTherapee (https://rawtherapee.com/) for post-processing adjustments. Considering that the underwater acquisition took approximately 45 min, in constant light and water conditions, the editing settings used for enhancing the first image were applied to all the photographs in a batch process. Although these operations relied on simple manual editing for improving white

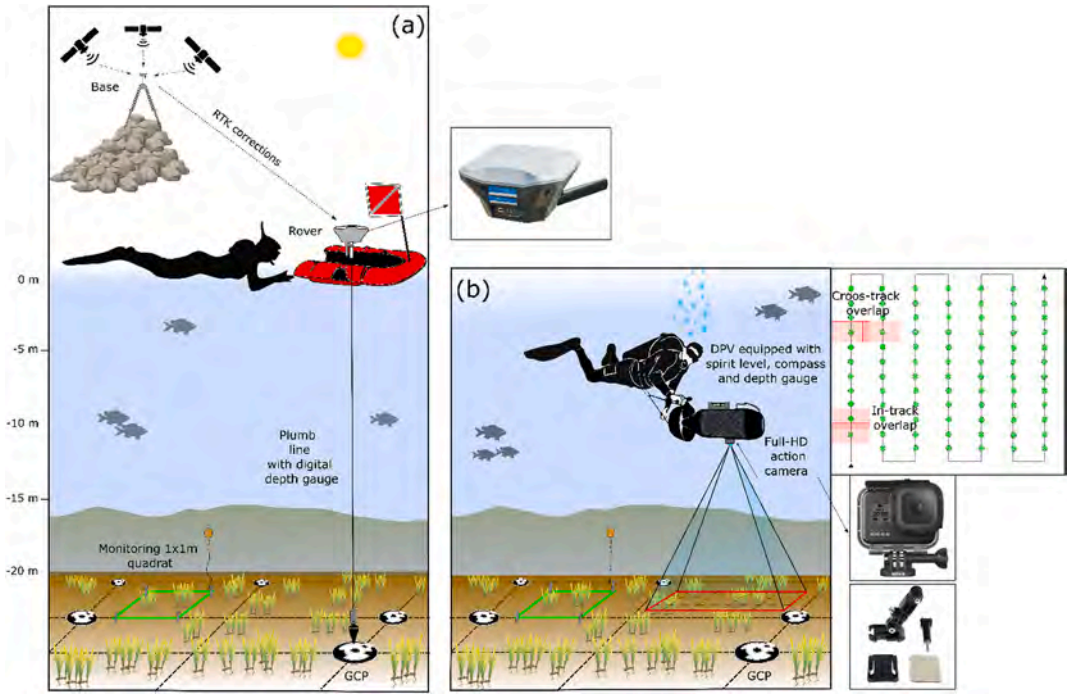

Fig. 2. Graphical layout of the equipment used for high-accuracy SfM-based mapping of seagrass transplantation (a) Permanent visible markers or ground control points (GCPs) and 1 × 1 m quadrats (in green) were placed on the seafloor inside the transplanting area, previously divided into 20 sub-plots by a 5 × 5 m grid (black dotted line). From the surface, XY and (-Z = depth) coordinates perpendicular to the vertical plane of each GCP were determined by a snorkelling operator using a low-cost RTK GNSS system and a plumb line equipped with a digital depth gauge. (b) The image acquisition was carried out by a SCUBA diver operator aided by a diver propulsion vehicle (DPV) equipped with a GoPro Hero 5 Black action camera. The inset in figure b shows the survey grid followed by the diver for a large-scale survey. The camera's position (green dots), images in-track and cross-track overlaps (red frames) are also shown, as well as the action camera and the adjustable adhesive mount used. (For interpretation of the references to color in this figure legend, the reader is referred to the Web version of this article.)

balance (change chromatic dominance by removing dominant greenish), contrast, shadow/highlight, saturation, and sharpening (removal of noise, edge enhancement) and were not supported by specific algorithms (Bryson et al., 2016) they could increase the probability of automatically detecting homologous points during photo alignments in SfM processing (Guidi et al., 2014).

2.6. Photogrammetric images processing

Data processing was carried out using SfM algorithms through Agisoft Metashape v 1.6.2 (Agisoft LLC, Russia), a low-cost (an affordable educational licence is available for institutions) commercial 3D reconstruction software which is widely used in the scientific community and does not require a very high level of expertise in stereo-photogrammetry. Despite the algorithms used to process the images not being public, the different steps of the process are configurable and can be controlled by the user to optimise the processing of imagery (Burns et al., 2019). For a more detailed discussion on SfM techniques, please refer to (D'Urban Jackson et al., 2020; Marre et al., 2019). To reduce errors due to fish-eye lenses typical of GoPro action cameras, camera calibration parameters such as the coordinates of the centre of projection of the image, the radial lens distortion coefficients and, non-linear distortion coefficients were estimated in Metashape by oblique underwater images representing a printed calibration chessboard reported in Fig. 1 of supporting material (SM). After images alignment, each ~500 m^2 sparse point cloud model (representing the site before and after *Posidonia* transplantation) was based on the alignment of approximately 800–1000 overlapping digital images. The "gradual selection" tool was used to remove the points in the sparse cloud presenting a high reconstruction uncertainty (e.g. *Posidonia* leaves which small movements occurred even in low current conditions). The criterions used to filter tie points were the reprojection error (Level aim = ~0.5), reconstruction uncertainty (Level aim = ~30) and, projection accuracy (Level aim = ~10).

Subsequently, the density of sparse point clouds was enhanced by Multi-View Stereo (MVS) algorithms. This process resulted in a dense XYZ point cloud between 23 and 30 million points. After manual detection of reflective GCPs, each cloud was scaled to real-world XYZ coordinates by adding GNNS coordinates to each GCPs with the "import reference" tab. A manual point cloud classification was carried to assign specific points to labelled groups such as vegetation, rocks, etc. Subsequently, by excluding such groups we exported clean clouds that represented only seabed features linked to transplantation (i.e. by removing external features such as clump weights and rocks). The dense point (Fig. 2a–c SM) could be converted into a texturized Delaunay Triangulated Irregular Network wireframe mesh (Fig. 2b SM) to support the generation of digital elevation models (DEMs) and orthophoto mosaics (Fig. 2d SM). The main steps adopted in our approach and the suggested parameters are reported in a graphical workflow (Fig. 3).

2.7. Accuracy assessment of 3D products

To check the quality of the 3D reconstructions, we rendered some artificial objects in the underwater scene and compared their known dimensions to dimensions estimated from the 3D model. The accuracy of a measurement was expressed with the following formula (Young et al., 2017): (Accuracy%) = 1- [|Object length [3D] - Object length [real]|/(Object length [real])]. In our test site, we used the linear lengths of 13 monitoring quadrats (1 × 1 m), the lengths and heights of underwater man-made structures (e.g., clump weights) and ten distances between GCPs measured *in situ* by a tape measure. Subsequently, a Spearman's rank correlation test was used to evaluate the association between real and estimated dimensions of objects. In addition, to evaluate the positional accuracy of georeferenced models we did not include

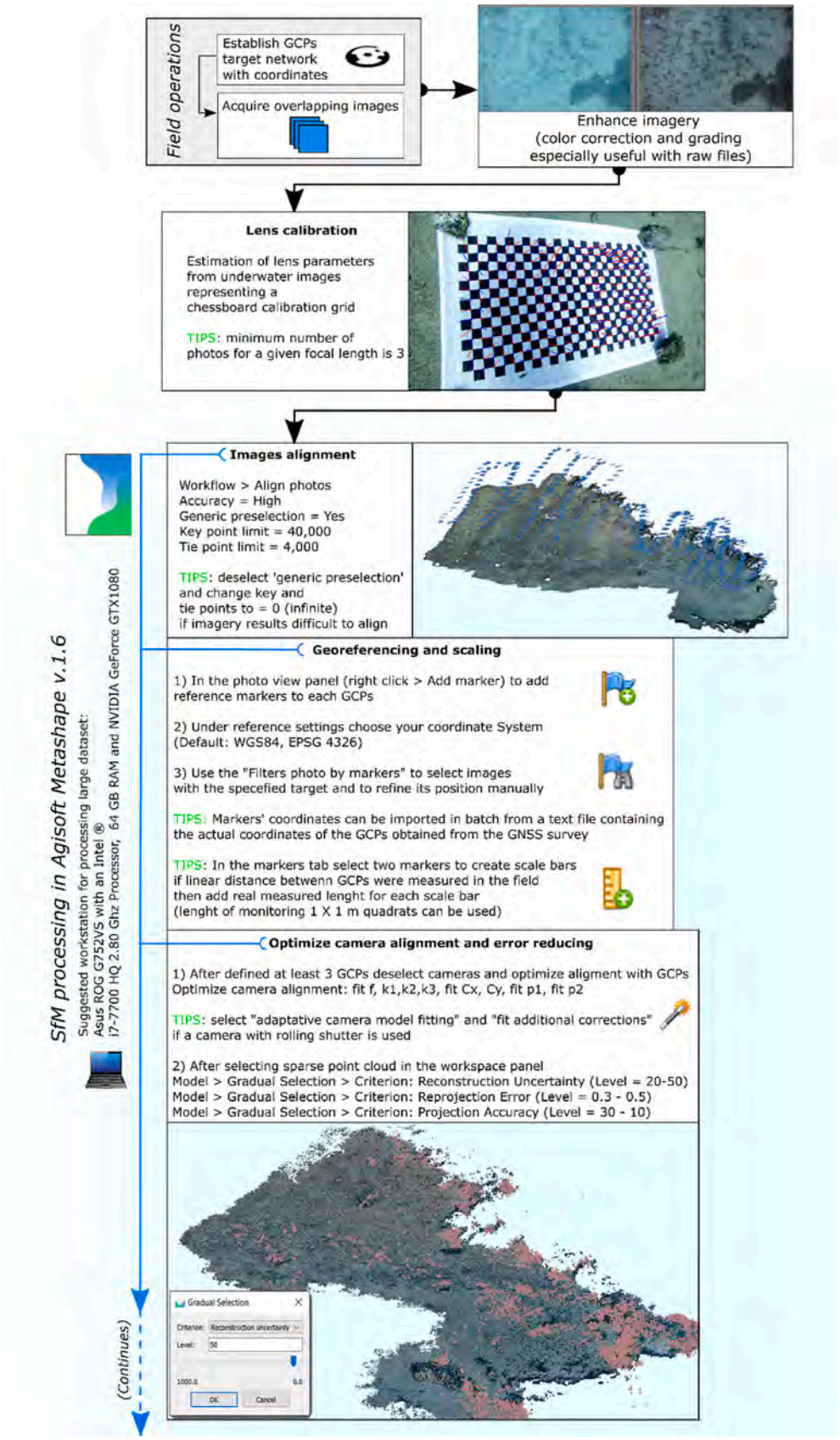

Fig. 3. Graphical workflow showing the main steps adopted in Agisoft Metashape v. 1.6 to create high spatial resolution and positionally accurate 3D point clouds, triangular meshes, and 2D raster outputs such as digital elevation models (DEMs) and orthophoto mosaics of transplantation seagrass areas, following initial overlapping photos and GCPs coordinates acquisitions. Icons are the same used in Agisoft Metashape toolbars to facilitate the reader during workflow application.

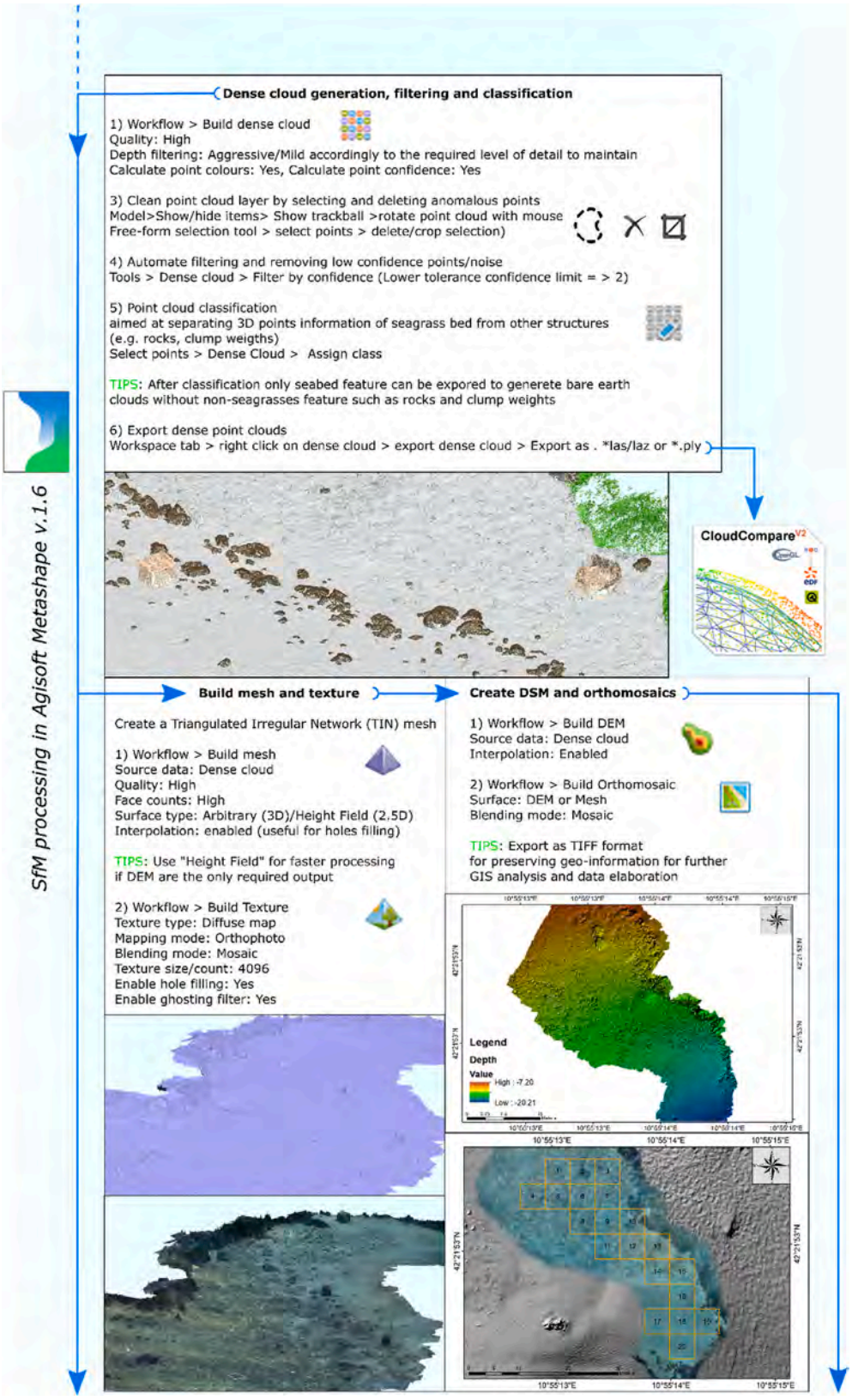

Fig. 3. (*continued*).

all the 15 surveyed GCPs in the photogrammetric processing during SfM workflow (bundle adjustment), but we used five of them as validation points (checkpoints, CPs) to assess the horizontal (x and y) and vertical (z) accuracies achieved after a bundle adjustment. Indeed, after unchecking the selected markers under the reference tab in Metashape, the Root Mean Square Error (RMSE) of these checkpoints was used to assess 3D scene reconstruction accuracy. The Root Mean Square Error (RMSE) was computed along the x-direction as: $RMSE_x =$

$\sqrt{\frac{1}{n}\times\sum_{i=1}^{n}(X_{Sfm_i})-(X_{GNSS_i})^2}$ where X_{SfM} indicates the coordinate estimated from the SfM process, whereas X_{GNSS} refers to the CPs coordinates measured with GNSS technique. Analogously, the RMSE was calculated on the y and z directions, and the total RMSE was estimated as: $RMSE_{total} = \sqrt{(RMSE_x^2)+(RMSE_y^2)+(RMSE_z^2)}$. Small values of RMSE indicate good quality of image alignment processes and block adjustments. Evaluating the accuracy of a georeferenced model using only GCPs is not fully objective since the shape of the model adapts to the GCPs, and consequently, GCPs will always achieve the lowest residuals. Using checkpoints (CP) provides a more objective quantification of the true accuracy of georeferencing procedures (Sanz-Ablanedo et al., 2018). Finally, seventh depth profiles of the seabed before the beginning of transplant operations were derived from high-resolution multibeam echosounder (MBES) acoustic bathymetry (derived from a hull-mounted RESON Seabat 7125 SV2) and compared to SfM-based DEM of the area.

2.8. Transplanted fragments monitoring over time

To examine the number and size of transplanted fragments and estimate their percent (%) cover and densities, RGB ortho-rectified photomosaics were imported in eCognition Developer 9 (ec), to perform a semi-automated image classification routine relying on object-based image analysis (OBIA) approach. After band normalization and median filtering algorithm, used to reduce noise and to improve the texture of the image objects (Som-ard et al., 2018), a multi-resolution segmentation (scale parameter = 80, shape = 0.5, compactness = 0.8) was adopted to grouping pixels into homogeneous regions (objects) based on their spectral differences due to red (R), green (G), and blue (B) bands. Even if the used parameters were specific for the segmentation process of our imagery, they can be used as starting values also for other applications implying the use of RGB high-resolution products. Subsequently, the 'Assign Class' algorithm was used to determine whether an image object belongs to a cover class, depending on threshold conditions. To distinguish the spectral signature of *Posidonia* fragments from sand and *matte* classes, we used as thresholds values both visible brightness [VB = (B + R + G)/3) and the Visible-band Difference Vegetation Index [VDVI = (2*G - R–B)/(2*G + R + B)] which is commonly used in crop-mapping applications to extract green vegetation (Wan et al., 2018). Finally, the pixel area (comprised between 1600 and 12,000 pixels) of classified objects as "*Posidonia* leaves", was used to separate fragments from other large, vegetated features such as natural patches of *Posidonia*. The accuracy of this semi-automatic detection of transplanted fragments was assessed using 13 monitoring quadrats in which direct counts were previously carried out by SCUBA operators.

2.9. Estimation of fragments height by topographic change detection

Considering that the estimation of the height of transplanted plants fragments is a useful metric to follow over time the growth of seagrasses due to their extension of leaves and rhizomes, we used a topographic change detection routine to compare height changes between before/after transplantation point clouds. Unfortunately, the achieved global accuracy of point clouds were not sufficient for a direct comparison of the elevations and accurate 3D change detection analysis using only GCPs information because both the error in the GNSS measures (some GCPs used for the georeferencing are re-surveyed since they have moved during transplant activities and storm events) and inaccuracies in the manual identification of markers on the images carried out in Metashape. Therefore, a co-registration of the "after" point cloud adopting as reference the "before" cloud was carried out. This step which is often needed in multi-temporal 3D models (Cucchiaro et al., 2018; Williams et al., 2018) and was performed using the powerful software CloudCompare v. 2.12 (http://www.cloudcompare.org/) which is an open-source solution to align and compare multiple 3D point clouds (Esposito et al., 2017). Fine alignment of the 3D point clouds representing the seabed before and after the transplanting operation implied a two-step process: (1) a rough alignment was performed using the 'point pairs' picking tool to select four matching pairs of points in each cloud, followed by (2) a fine registration, using an Iterative Closest Point (ICP) algorithm (Burns et al., 2016). In particular, the ICP algorithm was performed on a subset of the point clouds, corresponding to stable areas (e.g. rocks, clump weights), and then the obtained rigid transformation matrix was applied to the whole original point clouds. For this study, a minimum RMS improvement between 2 consecutive iterations of 1×10^{-5} m was used and the minimum iterations were set to 1000 to ensure that the improvement threshold was met first. To speed up the processing time and to avoid working on large clouds, we segmented the point clouds (with the interactive segmentation tool in CloudCompare) in smaller areas using a shapefile representing the working grid (5 × 5 m frames) adopted to sectorise the transplanting area. Multitemporal geomorphic changes in the transplant area were identified by comparing the co-registered SfM-derived 3D point clouds. For each point cloud, vertical (+Z) distances were estimated with the multiscale model-to-model cloud comparison (M3C2) algorithm (Lague et al., 2013) according to the procedure reported in (James et al., 2017b, 2020, 2017b) based on precision maps (PM), to highlight areas of significant change due to the newly transplanted fragments. The output from M3C2-PM represented 3D change between "before" and "after" point clouds along with local normal directions, along with an assessment of whether that change exceeded the local level of ($LoD_{95\%}$), derived from the 3-D spatially variable photogrammetric and georeferencing precision maps. Point coordinate precision estimates for the sparse point cloud were exported from Metashape to a text file by a Python script provided in James et al. (2020). CloudCompare was then used to interpolate such sparse point cloud 3D precision estimates across the dense point clouds using the 'nearest neighbours' option under the 'scalar field' toolbar. More details regarding the specific software settings and the principle of the M3C2 algorithm are reported in the supplementary material (Fig. 3 SM).

2.10. Estimation of the effects of transplanting operation on the seabed

Because ecological restoration aims to restore both degraded habitats and the ecosystem's functioning, seagrass restoration effects on the physical and biological features of surrounding habitats should be also assessed. To estimate fine-scale changes in seabed morphology due to transplantation of *Posidonia* fragments, aligned point clouds were exported as 2D raster grids (single band GeoTIFF files) with the 'rasterize tool' in CloudCompare and analysed in ESRI® ArcGIS software to detect changes in the seabed vector ruggedness measure or VRM [see Benthic Terrain Modeller tool for ArcMap (Walbridge et al., 2018),].

3. Results

3.1. Accuracy assessment of 3D products

Following our protocol, we reported that the underwater measures derived by 3D models matched strongly with their true dimensions as demonstrated by a significant positive correlation (Spearman's rho = 0.95, S = 28.602, p-value < 0.0001) between object length [real] and object length [3D], resulting in a mean accuracy of 99.55% (±0.03 SD). As a proxy of the internal quality of the bundle adjustment of the image block, we used the RMSE of residuals at checkpoints. For each model (study area before and after transplantation), the RMSE in planimetry (X and Y) and the RMSE in altimetry (Z) of residuals at checkpoints (CPs). In both cases, centimetric accuracy was reached (Table 1) but for the model concerning the *scenario* after transplantation, we obtained larger RMSE because of the removal of 3 GCPs due to the effects of waves during bad weather. The comparison between high-resolution (~2 cm)

Table 1
Positional accuracy of cartographic products (orthophoto images) after bundle block adjustment expressed as RMSE of the residuals at ground control points (GCPs) and checkpoints (CPs).

SfM point cloud dataset		Count	Control points RMSE				
			X error (cm)	Y error (cm)	Z error (cm)	XY error (cm)	Total (cm)
Before transplantation (May 2020)	**GCPs**	10	4.538	4.213	5.336	6.192	8.174
Number of points: 27,303,919 Point density: 37,005 points/m^2	**CPs**	5	6.668	4.555	1.597	8.076	9.053
After transplantation (September 2020)	**GCPs**	7	20.229	19.854	3.726	18.344	18.588
Number of points: 48,753,741 Point density: 35,499 points/m^2	**CPs**	5	21.300	10.037	1.597	23.546	23.600

DEM derived from SfM workflow and MBES bathymetry revealed a mean difference in height of 0.18 m (±0.3 SD) among the seven depth profiles analysed (Fig. 4).

3.2. Monitoring of transplanted fragments

The use of RGB bands and derived index (VB and VDVI) during OBIA processing of SfM derived high-resolution orthophotomosaics allowed a good separation of *Posidonia* cutting from the other two seabed cover classes (dead *matte* and sand, Fig. 5). At the end of transplantation, we reported an overall classification accuracy for fragments of 86.15% assessed in the 13 monitoring quadrats, used as ground truth data (Fig. 6). After one year (at the end of field works in summer 2020), the total transplantation area (490 m^2) was vegetated with 3840 fragments of *P. oceanica,* corresponding at 8.5 fragments/m^2. The mean surface area for each cutting was 85 cm^2 (±0.04 SD), resulting, at the end of transplanting, in an increase in percentage cover from 0% to 9.28% over the whole area (Fig. 7).

3.3. Topographic change detection of post-transplantation seabed

For the alignment process, the before-transplantation point cloud was used as the fixed reference and the after-transplantation cloud was transformed to the best fit. The final RMS error after the fine registration process with the ICP algorithm was: 0.010083 (computed on 40,000,000 points).

Significant changes between the two-point clouds were reported in all the twenty 5 × 5 m frames. In stationary conditions of the seabed (i.e. without major erosion and accumulation events), positive values along the +Z axis can be regarded as a good proxy of fragments' height (Figs. 8 and 4 SM). We reported that most of the transplanted fragments (>85%) led to a change in seabed vertical topography (along the +Z axis) due to their lengths which were comprised between 6 and 20 cm (Fig. 5 SM).

Finally, also 2D raster analysis confirmed a clear increase of the VRM values on sandy areas, directly linked to the presence of transplanted fragments which influenced terrain complexity (Fig. 9). By excluding from computation, the edge of the natural meadow, the mean values of VRM before the transplantation were 0.23 (±0.17 SD) which increased up to 0.42 (±0.22 SD) after the transplantation of *Posidonia* fragments.

4. Discussions

Protection and restoration are crucial components of conservation strategies aimed at preserving both biodiversity and ecosystem services

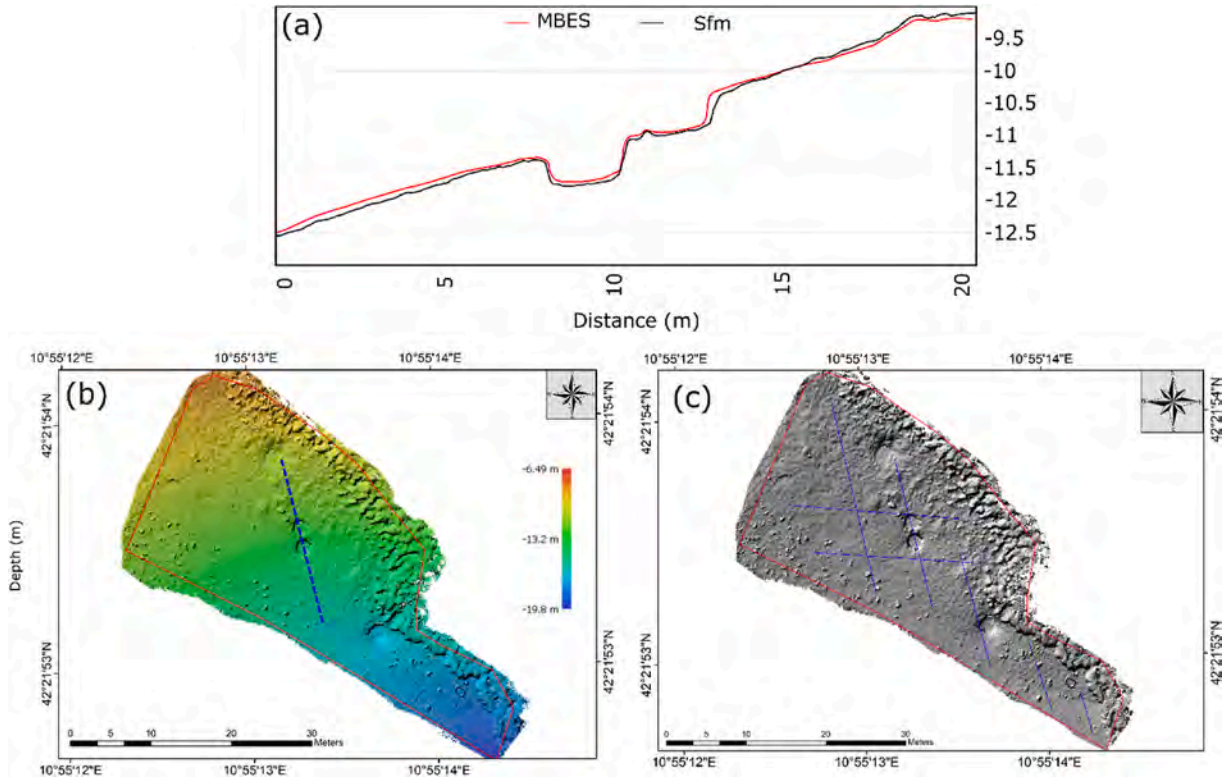

Fig. 4. (a) Comparison of the topographic profiles derived from SfM-based DEM and MBES-based bathymetrySfM-based DEM is shown both as colorized grid (b) and shaded relief (c). The dotted blu line in b represents the depth profile reported in a, whilst in c the other six depth profiles used in the estimation of mean height differences are shown.

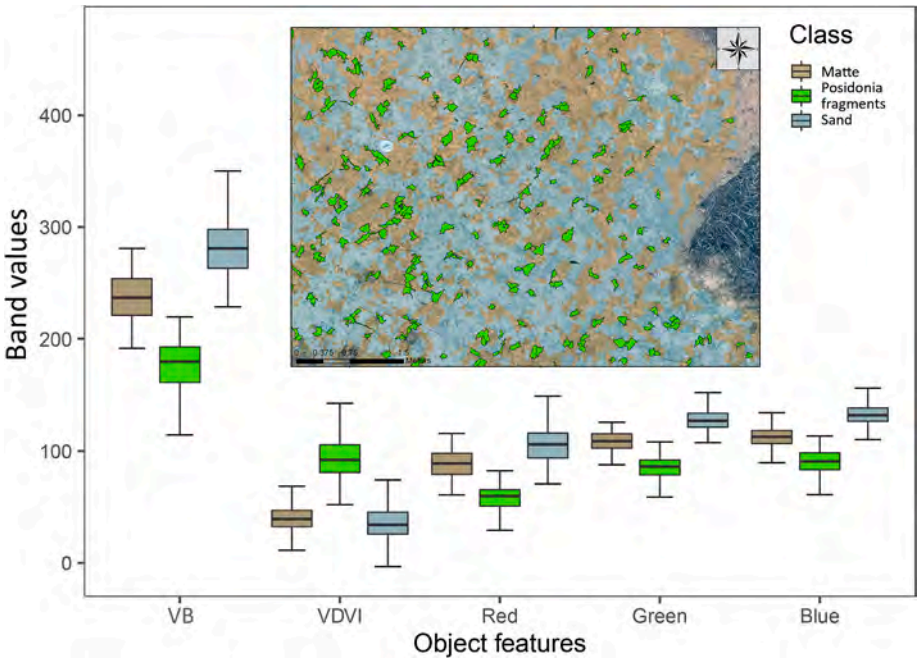

Fig. 5. Boxplots showing the differences in band values (RGB) and their derived index (VB = visible brightness and VDVI = Visible-band Difference Vegetation Index) of seabed cover classes defined during OBIA classification of the transplantation area. The map shows the polygons identfying *Posidonia* transplanted fragments (in light green) after segmentation and classification steps. *Posidonia* fragments are clearly separated from the other seabed cover classes (matte and sand). (For interpretation of the references to color in this figure legend, the reader is referred to the Web version of this article.)

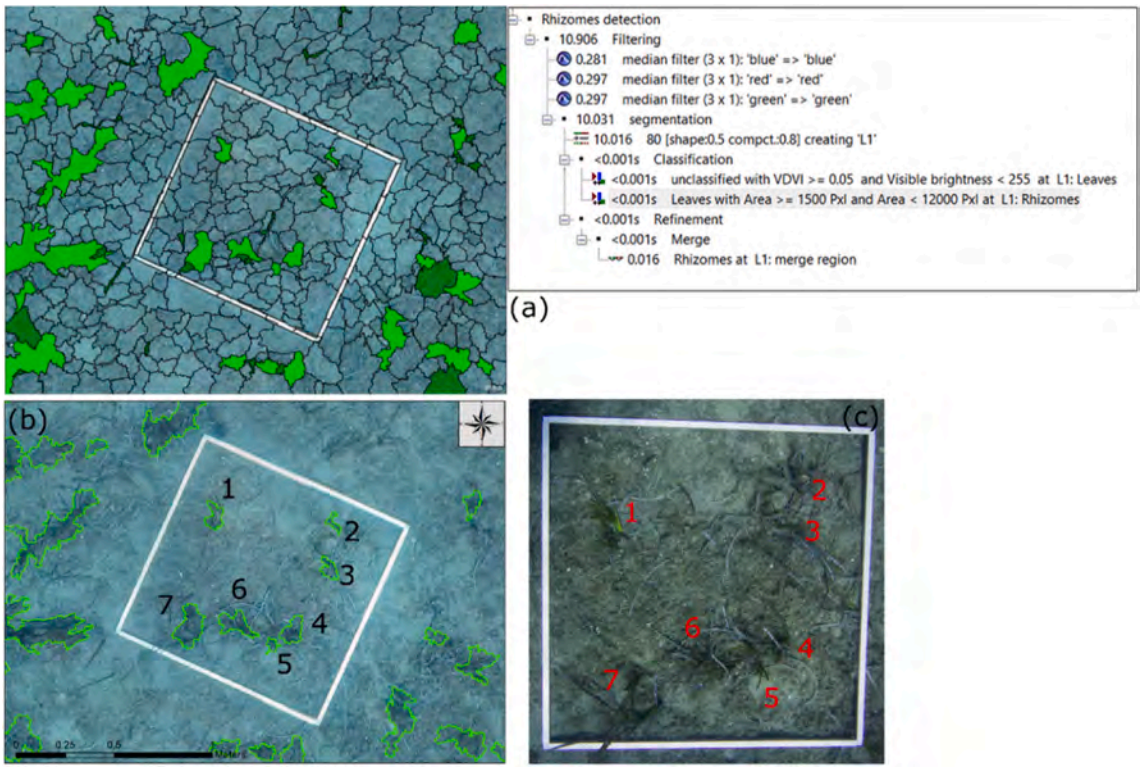

Fig. 6. Image segmentation processes aimed at extracting and counting polygon outlines surrounding the transplanted *Posidonia* fragments. (a) Image objects delineation after orthomosaic segmentation and the specific rule set developed in eCognition 9. (b) Classified segments visualized in ESRI ArcMap software. (c) Example of accuracy classification assessment. Underwater photo of the same monitoring quadrat reported in a and b used as ground truth data.

(Possingham et al., 2015). Because restoration actions imply repeated sampling events to assess both the conservation status and the transplanting performance, reliable, rapid and cost-effective monitoring methods are required to detect even slight modifications of the status of the transplanted meadows. Therefore, a key aspect is to accurately georeference the monitored data to ensure effective comparisons over time, making not technically suitable consumer-grade Global Positioning System (GPS) receivers which offer positional accuracy in the order of 3–10 m (Dodd, 2011). For this reason, acoustic-based surveys (MBES and Side Scan Sonar) carried out by surveying vessels are the most used for marine habitat mapping and monitoring large areas (Gumusay et al., 2019) being capable of providing accurate positioning of data through onboard GNSS receivers that usually combine high-quality antennas with multiple band reception (L1, L2 or L5).

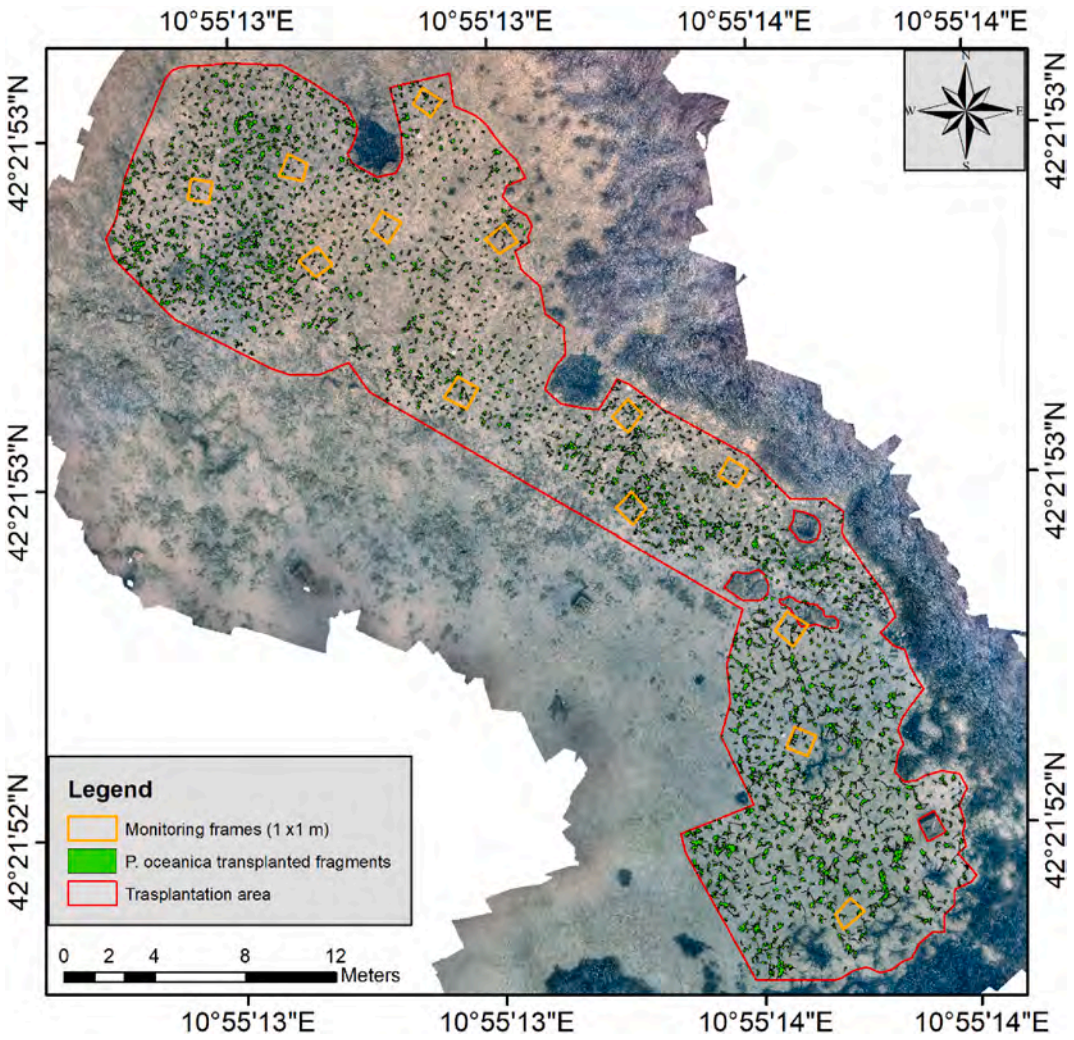

Fig. 7. RGB orthophotomosaic of the transplantation area (red outline) at the end of September 2020 showing the transplanted *P. oceanica* fragments (green polygons) and the monitoring 1 × 1 m quadrats (in orange) used to assess the accuracy of OBIA classification. (For interpretation of the references to color in this figure legend, the reader is referred to the Web version of this article.)

However, such instruments are in general with dimensions and power requirements that can pose problems to be used on small size platforms (Matias et al., 2015) and have high operational costs (Survey-grade GNSS systems often exceeding $20,000 for the two devices needed) resulting prohibitive for many research needs. For the aforementioned reasons, we describe the use of lightweight single frequency (L1) and low-cost RTK GNSS units to create highly accurate underwater photogrammetric deliverables. The equipment adopted in our work can be regarded as a starting point for other applications which require high positional accuracy with reasonable costs. The large diffusion of low-cost GNSS devices along with the wide range of deployment and open source post-processing solutions (Takasu and Yasuda, 2009), will revolutionize spatial ecology making these systems an important new tool for a variety of applications (Hill et al., 2019). Another main limitation of traditional acoustic techniques is the mismatch between the pixel resolution of sensors and the scale of ecological processes. This is especially true in seagrass restoration programmes where the success of such interventions can be evaluated by fine-scale monitoring aimed at estimating the survival of transplanted plants (e.g., fragments, seedlings, or rhizomes). In these cases, most of the biological descriptors used in seagrass monitoring such as shoot density, Leaf Area Index (LAI), Daily Leaf Production (DLP), rhizome elongation, require a direct interaction between SCUBA operators and plants, leading to safety and operational constraints such as gas supplies, the extent of the surveyed area, operator subjectivity. Therefore, as reported in other imagery-based applications for seagrass mapping (Marre et al., 2020; Mohamed et al., 2020; Rende et al., 2015) we also aimed to develop an efficient operational methodology that is automatic and reproducible for fine-scale mapping applications in which other useful metrics such as percent cover, number of fragments and canopy height can be estimated from SfM products. These metrics other than providing an effective evaluation on the status of transplantation can be also used to evaluate patchiness (i.e. aggregation of multiple plagiotropic fragments over time) to follow the natural re-colonisation and growth of the meadow (Bacci et al., 2017). Our protocol is well suitable in almost all seagrass restoration projects facing the problem of shifting the state of the seafloor from an unvegetated to a vegetated habitat. So far, restoration projects were characterized by a reduced number of fragments/m^2 due to the scarce availability of vegetal material to be transplanted (van Katwijk et al., 2016). In fact, in such circumstances, the low densities of transplanted plants and the relatively low number of leaves ensure good results during images alignment and tie points detection (Marre et al., 2020).

GoPro action cameras are becoming a valuable tool for underwater acquisition because, despite some weaknesses, such as quite a large radial distortion due to wide-angle, small focal length, and limited control of manual settings, they provide an easy, low-cost, and lightweight way for non-expert personnel to acquire underwater images due

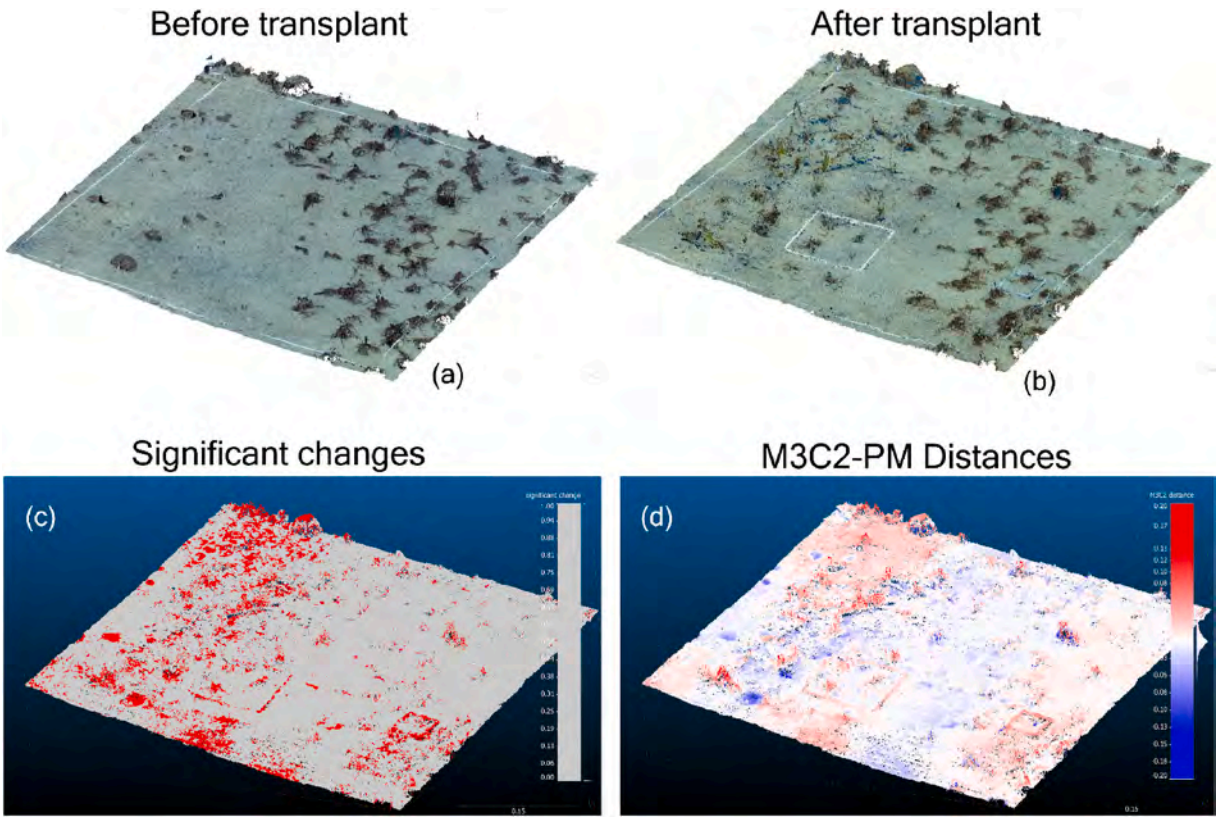

Fig. 8. Estimation of topographic change detection of the seabed after transplantation of *Posidonia* fragments carried out in a 5 × 5 m frame using CloudCompare (M3C2-PM plugin). (a) 3D dense point cloud before completing transplantation. Note that half of the frame presented a bare sandy bottom whilst the other half was already vegetated with *Posidinia* fragments (b) 3D dense point cloud after further transplanting operations. (c) Areas where significant elevation changes occurred are highlighted in in red. (d) Computed distances between the two points clouds (before and after transplant) along the +Z axis. Positive values (in red) are related to the presence of transplanted fragments (top left corner), slight sediments accumulation, and some objects used during transplant activities (metallic frames). Blue areas with negative values depend on the removal of pebbles or from the lacking positions of benthic organisms (sea cucumbers *Holothuria tubulosa*). (For interpretation of the references to color in this figure legend, the reader is referred to the Web version of this article.)

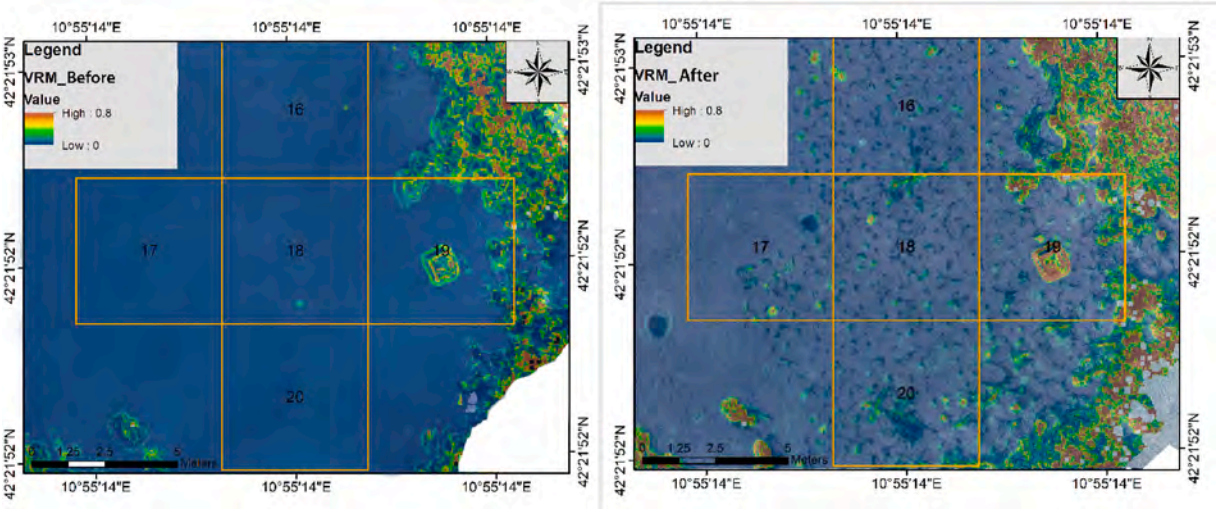

Fig. 9. 2D raster maps showing vector ruggedness measure values (VRM) estimated at 3 cm per pixel neighbourhood size over 25 m^2 (5 × 5 m frames from n. 16 to 20, at 18 m depth). High VRM values are highlighted in red, whilst low values are in blue. (For interpretation of the references to color in this figure legend, the reader is referred to the Web version of this article.)

to their default settings (Raoult et al., 2016). The acquisition parameters used are should be considered as starting point for other applications being directly derived from our field tests with a non-metric camera. However, if greater details and pixel resolution are required to better characterize plants attributes, professional Digital Single Lens Reflex (DSLR) cameras with larger image sensors (ideally full-frame ≥ 1″ with global shutters) can be used to improve results. Such cameras can be equipped with specific low distortion lenses and underwater housing

with a hemispheric dome port capable of significantly reducing water refraction and distortion, improving the ability of software to accurately align the images (Menna et al., 2018).

Regarding SfM imagery processing, the software used for creating accurate 3D models typically falls into one of two categories: 1) commercially available software (Agisoft Metashape, Pix4D, Autodesk ReCap Photo, Photomodeler, 3D Zephyr), for which the workflow is more streamlined and expert supervision is unnecessary, but is a 'black box' and allows limited control by the user on 3D reconstruction processes, and 2) open-source software (Bundler, VisualSFM, OpenDroneMap, Meshroom, COLMAP, PPT GUI, Regard 3D), which allows more involvement by the user during data processing, but the workflow is usually more complex (several programs may not have a graphical user interface [GUI]). Similar considerations apply for OBIA processing that recently has emerged as a new paradigm for managing spectral variability in ultra-high (<1 cm/pixel) spatial resolution images, replacing pixel-based approach by working with groups of homogeneous and contiguous pixels as base units to perform classification, reducing the intra-class spectral variability of classic pixel-oriented methods. Even if our approach implied the use of professional software (eCognition) that due to license costs could be restricted to a limited group of operators, also open-source software packages for geospatial analysis with OBIA algorithms are available, such as the Orfeo ToolBox (OTB), developed by the French Centre National d'Etudes Spatiales (CNES). OTB can be operated either autonomously or through a second open-source software (i.e., QGIS), used as a graphical interface that enables a graphical analysis of data processing (De Luca et al., 2019). One of the main limitations of the OBIA approach is that it is highly dependent on the kind of imagery and the user experience, and will likely vary even among experienced analysts and datasets (Hulet et al., 2014). Moreover, similarly to SfM processes, OBIA analysis carried out on large raster datasets can be demanding of both RAM and video cards, so computer processing power limitations and time constraints should also be considered when large areas have to be monitored in a relatively short timeframe. Challenges remain in forecasting the achievable accuracy of output topographic survey (Wheaton et al., 2010) due to measurement 'accuracy' (associated with systematic error or bias) and 'precision' (describing random error). However, with the approach (M3C2-PM) suggested by James et al. (2017b, 2020), confidence-bounded change detection based on precision maps can be assessed from SfM-based surveys. In fact, in the native M3C2 algorithm, measurement precision is estimated from local surface roughness, which is highly appropriate for the Terrestrial Laser Scanners (TLSs) data for which it was primarily designed (James et al., 2017b). However, purely roughness-based precision estimates are unlikely to be representative of uncertainty in photogrammetric point clouds where errors in adjacent point positions will be highly correlated due to the bundle adjustment process (James et al., 2017b). In addition, the smoothing or filtering incorporated into image matching algorithms can strongly mute the representation of small-scale roughness in photo-derived point clouds (James et al., 2020). For this reason, M3C2-PM variant which uses 3-D precision estimates from associated precision maps should be used for SfM-derived point clouds (where roughness can be a poor measure of precision).

Besides, like other SfM-based photogrammetric applications used in coral reef ecology (Price et al., 2019) relying on underwater photos acquisition, local factors may affect the results such as water turbidity and light intensity. These aspects might make this protocol inadequate for very turbid coastal environments or deep areas (>20 m). We were able to apply this protocol from 10 up to 22 m, a depth interval which in our study site showed a light range comprised between approximately 18,300 ± 6800 and 9260 ± 4800 Lux (mean values estimated from PAR value measured with CTD probe during the summer season at 10 and 20 m depth). However, seagrass meadows develop in shallow and light environments, and transplantations are usually carried out in such habitats (Van Katwijk et al., 2009). The acquisition of GCP coordinates by snorkel operators working from the surface imply extremely calm conditions and the absence of currents to avoid errors in the measurement with the plumb bob and RTK systems. It should be noted that the number and arrangement of GCPs could have considerable effects on results, therefore dense deployments of carefully measured GCPs represent a substantial part of the overall survey effort (James et al., 2017a). Therefore, the level of repeatability/comparability across outputs may vary accordingly to cameras, operators, markers used and sea conditions, and should be carefully assessed to be minimised (Bayley and Mogg, 2020). Last but not the least, new advances in DPV systems, action cameras, and SfM processing will allow the 3D reconstruction of huge areas, as we reported from a field test carried out in July 2021 where 3200 m^2 were successfully mapped by using a GoPro Hero 9 action camera, through a 1h 10' minutes dive (high-resolution KMZ file is provided within supplementary material).

5. Conclusions

Despite these existing drawbacks, the workflow presented allowed the precise monitoring of seagrass transplantation using fast and low-cost technology. 3D modelling and mapping using SfM algorithms, capable of capturing and storing huge amounts of information on the substrate and at the community level may provide great potential for effectively monitoring restored seagrass beds, detecting small changes in seabed topography on a large scale. When fast and recurring monitoring programmes are required (e.g after a storm events) or when "before" data are not available, only 2D raster outputs could be used to precisely map the transplantation areas and check the percent cover of transplanted seagrass fragments through OBIA classification. Because seagrass restoration has become a common management tool for recovering the ecological functions and services lost due to habitat fragmentation and degradation, this workflow will provide a methodological platform for optimizing resources in future seagrass restoration policies and serve as a proof of concept aimed at implementing this cost-effective and non-intrusive monitoring method as a standard tool within the management of transplantation programmes.

Authorship contribution statement

D.V., G.M., E.C.: Conceptualization, Methodology, Data acquisition; DV: Data acquisition, Formal analysis, Software implementation, Writing - original draft; G.M., E.C., D.S.P, G.J.L.: Writing - review and editing; A.B., G.D.A.: Methodology, Conceptualization, Supervision, Project administration, Funding acquisition; G.D.A. scientific coordinator of the transplantation activities.

Declaration of competing interest

The authors declare that they have no known competing financial interests or personal relationships that could have appeared to influence the work reported in this paper.

Acknowledgements

We would like to thank the National Geographic Society (grant #EC-173R-18) for initial funding support which allowed the purchase of part of the equipment used. We are indebted to three anonymous reviewers and Editor for their valuable comments that have considerably improved the manuscript.

Appendix A. Supplementary data

Supplementary data to this article can be found online at https://doi.org/10.1016/j.jenvman.2021.114262.

References

Abadie, A., Boissery, P., Viala, C., 2018. Georeferenced underwater photogrammetry to map marine habitats and submerged artificial structures. Photogramm. Rec. 33, 448–469. https://doi.org/10.1111/phor.12263.

Asriani, N., Ambo-Rappe, R., Lanuru, M., Williams, S.L., 2018. Species richness effects on the vegetative expansion of transplanted seagrass in Indonesia. Bot. Mar. 61, 205–211.

Bacci, T., Rende, F.S., Scardi, M., 2017. Shoot micro-distribution patterns in the Mediterranean seagrass Posidonia oceanica. Mar. Biol. 164, 85.

Balestri, E., Vallerini, F., Lardicci, C., 2011. Storm-generated fragments of the seagrass Posidonia oceanica from beach wrack–A potential source of transplants for restoration. Biol. Conserv. 144, 1644–1654.

Bastyan, G.R., Cambridge, M.L., 2008. Transplantation as a method for restoring the seagrass Posidonia australis. Estuar. Coast Shelf Sci. 79, 289–299. https://doi.org/10.1016/j.ecss.2008.04.012.

Bayley, D.T.I., Mogg, A.O.M., 2020. A protocol for the large-scale analysis of reefs using Structure from Motion photogrammetry. Methods Ecol. Evol. 11, 1410–1420. https://doi.org/10.1111/2041-210X.13476.

Bayley, D.T.I., Mogg, A.O.M., Koldewey, H., Purvis, A., 2019. Capturing complexity: field-testing the use of "structure from motion" derived virtual models to replicate standard measures of reef physical structure. PeerJ 2019 1–17. https://doi.org/10.7717/peerj.6540.

Boudouresque, C.F., Bernard, G., Pergent, G., Shili, A., Verlaque, M., 2009. Regression of Mediterranean seagrasses caused by natural processes and anthropogenic disturbances and stress: a critical review. Bot. Mar. 52, 395–418. https://doi.org/10.1515/BOT.2009.057.

Bryson, M., Johnson-Roberson, M., Pizarro, O., Williams, S.B., 2016. True color correction of autonomous underwater vehicle imagery. J. Field Robot. 33, 853–874.

Burns, J.H.R., Delparte, D., Kapono, L., Belt, M., Gates, R.D., Takabayashi, M., 2016. Assessing the impact of acute disturbances on the structure and composition of a coral community using innovative 3D reconstruction techniques. Metods Oceanogr. 15–16, 49–59. https://doi.org/10.1016/j.mio.2016.04.001.

Burns, J.H.R., Fukunaga, A., Pascoe, K.H., Runyan, A., Craig, B.K., Talbot, J., Pugh, A., Kosaki, R.K., 2019. 3D Habitat complexity of coral reefs in the Northwestern Hawaiian Islands is driven by coral assemblage structure. ISPRS - Int. Arch. Photogramm. Rem. Sens. Spat. Inf. Sci. XLII-2/W10, 61–67. https://doi.org/10.5194/isprs-archives-XLII-2-W10-61-2019.

Casoli, E., Mancini, G., Ventura, D., Belluscio, A., Ardizzone, G., 2021. Double trouble: synergy between habitat loss and the spread of the alien species Caulerpa cylindracea (sonder) in three Mediterranean habitats. Water 13, 1342.

CloudCompare (Version 2.12) [GPL Software], 2020. Retrieved from. http://www.cloudcompare.org/.

Cucchiaro, S., Maset, E., Fusiello, A., Cazorzi, F., 2018. 4D-SFM photogrammetry for monitoring sediment dynamics in a debris-flow catchment: software testing and results comparison. In: 2018 ISPRS TC II Mid-term Symposium" towards Photogrammetry 2020. International Society for Photogrammetry and Remote Sensing, pp. 281–288.

Cunha, A.H., Marbá, N.N., van Katwijk, M.M., Pickerell, C., Henriques, M., Bernard, G., Ferreira, M.A., Garcia, S., Garmendia, J.M., Manent, P., 2012. Changing paradigms in seagrass restoration. Restor. Ecol. 20, 427–430.

De Luca, G., N Silva, J.M., Cerasoli, S., Araújo, J., Campos, J., Di Fazio, S., Modica, G., 2019. Object-based land cover classification of cork oak woodlands using UAV imagery and orfeo toolbox. Rem. Sens. 11, 1238.

Delgado, O., Pérez, M., Ruiz, J.M., Ballesteros, E., Romero, J., 1999. Effects of fish farming activities on seagrass (Posidonia oceanica) beds in a Mediterranean bay: seagrass decline post-disturbance. Oceanol. Acta 22, 110–117.

Dodd, M., 2011. Where are my quadrats? Positional accuracy in fieldwork. Methods Ecol. Evol. 2, 576–584.

Duarte, C.M., 2002. The future of seagrass meadows. Environ. Conserv. 29, 192–206.

Duarte, C.M., Marbà, N., Gacia, E., Fourqurean, J.W., Beggins, J., Barrón, C., Apostolaki, E.T., 2010. Seagrass community metabolism: assessing the carbon sink capacity of seagrass meadows. In: Global Biogeochem. Cycles 24. eCognition Developer, T., 2014. 9.0 User Guide. Trimble Ger. GmbH Munich, Ger.

D'Urban Jackson, T., Williams, G.J., Walker-Springett, G., Davies, A.J., 2020. Three-dimensional digital mapping of ecosystems: a new era in spatial ecology. Proc. R. Soc. B 287, 20192383.

Esposito, G., Salvini, R., Matano, F., Sacchi, M., Danzi, M., Somma, R., Troise, C., 2017. Multitemporal monitoring of a coastal landslide through SfM-derived point cloud comparison. Photogramm. Rec. 32, 459–479. https://doi.org/10.1111/phor.12218.

Francour, P., Ganteaume, A., Poulain, M., 1999. Effects of boat anchoring in posidonia oceanica seagrass beds in the port-Cros national park (north-western Mediterranean Sea). Aquat. Conserv. Mar. Freshw. Ecosyst. 9, 391–400. https://doi.org/10.1002/(SICI)1099-0755(199907/08)9:4<391::AID-AQC356>3.0.CO;2-8.

Guidi, G., Gonizzi, S., Micoli, L., 2014. Image pre-processing for optimizing automated photogrammetry performances. In: ISPRS Technical Commission V Symposium. ISPRS, pp. 145–152.

Gumusay, M.U., Bakirman, T., Tuney Kizilkaya, I., Aykut, N.O., 2019. A review of seagrass detection, mapping and monitoring applications using acoustic systems. Eur. J. Remote Sens. 52, 1–29.

Heck Jr., K.L., Hays, G., Orth, R.J., Heck, K.L., Hays, G., Orth, R.J., 2003. Critical evaluation of the nursery role hypothesis for seagrass meadows. Mar. Ecol. Prog. Ser. 253, 123–136. https://doi.org/10.3354/meps253123.

Hill, A.C., Limp, F., Casana, J., Laugier, E.J., Williamson, M., 2019. A new era in spatial data recording: low-cost GNSS. Adv. Archaeol. Pract. 7, 169–177.

Hulet, A., Roundy, B.A., Petersen, S.L., Jensen, R.R., Bunting, S.C., 2014. Cover estimations using object-based image analysis rule sets developed across multiple scales in pinyon-juniper woodlands. Rangel. Ecol. Manag. 67, 318–327. https://doi.org/10.2111/REM-D-12-00154.1.

Inglis, G.J., Smith, M.P.L., 1995. An examination of observer bias as a source of error in surveys of seagrass shoots. Aust. J. Ecol. 20, 273–281.

James, M.R., Robson, S., d'Oleire-Oltmanns, S., Niethammer, U., 2017a. Optimising UAV topographic surveys processed with structure-from-motion: ground control quality, quantity and bundle adjustment. Geomorphology 280, 51–66.

James, M.R., Robson, S., Smith, M.W., 2017b. 3-D uncertainty-based topographic change detection with structure-from-motion photogrammetry: precision maps for ground control and directly georeferenced surveys. Earth Surf. Process. Landforms 42, 1769–1788. https://doi.org/10.1002/esp.4125.

James, M.R., Antoniazza, G., Robson, S., Lane, S.N., 2020. Mitigating systematic error in topographic models for geomorphic change detection: accuracy, precision and considerations beyond off-nadir imagery. Earth Surf. Process. Landforms 45, 2251–2271.

Kalacska, M., Lucanus, O., Arroyo-Mora, J.P., Laliberté, É., Elmer, K., Leblanc, G., Groves, A., 2020. Accuracy of 3d landscape reconstruction without ground control points using different uas platforms. Drones 4, 13.

Klumpp, D.W., Nichols, P.D., 1983. A study of food chains in seagrass communities II. Food of the rock flathead, Platycephalus laevigatus Cuvier, a major predator in a Posidonia australis seagrass bed. Mar. Freshw. Res. 34, 745–754.

Lague, D., Brodu, N., Leroux, J., 2013. Accurate 3D comparison of complex topography with terrestrial laser scanner: application to the Rangitikei canyon (N-Z). ISPRS J. Photogrammetry Remote Sens. 82, 10–26. https://doi.org/10.1016/j.isprsjprs.2013.04.009.

Larkum, A.W.D., Orth, R.J., Duarte, C.M., 2006. Seagrasses: biology, ecologyand conservation. Phycologia 45, 5.

Mancini, G., Casoli, E., Ventura, D., Jona-Lasinio, G., Criscoli, A., Belluscio, A., Ardizzone, G.D., 2019. Impact of the Costa Concordia shipwreck on a Posidonia oceanica meadow: a multi-scale assessment from a population to a landscape level. Mar. Pollut. Bull. 148 https://doi.org/10.1016/j.marpolbul.2019.07.044.

Marre, G., Holon, F., Luque, S., Boissery, P., Deter, J., 2019. Monitoring marine habitats with photogrammetry: a cost-effective, accurate, precise and high-resolution reconstruction method. Front. Mar. Sci. 6, 1–15. https://doi.org/10.3389/fmars.2019.00276.

Marre, G., Deter, J., Holon, F., Boissery, P., Luque, S., 2020. Fine-scale automatic mapping of living posidonia oceanica seagrass beds with underwater photogrammetry. Mar. Ecol. Prog. Ser. 643, 63–74. https://doi.org/10.3354/meps13338.

Matias, B., Oliveira, H., Almeida, J., Dias, A., Ferreira, H., Martins, A., Silva, E., 2015. High-accuracy low-cost RTK-GPS for an unmannned surface vehicle. In: OCEANS 2015-Genova. IEEE, pp. 1–4.

Menna, F., Nocerino, E., Remondino, F., 2018. Photogrammetric modelling of submerged structures: influence of underwater environment and lens ports on three-dimensional (3D) measurements. In: Remondino, F., Georgopoulos, A., González-Aguilera, D., Agrafiotis, P. (Eds.), Latest Developments in Reality-Based 3d Surveying and Modelling. MDPI, Basel, Switzerland, pp. 279–303, 2018.

Mohamed, H., Nadaoka, K., Nakamura, T., 2020. Towards benthic habitat 3D mapping using machine learning algorithms and structures from motion photogrammetry. Rem. Sens. 12, 127.

Nex, F., Remondino, F., 2014. UAV for 3D mapping applications: a review. Appl. Geomatics 6, 1–15. https://doi.org/10.1007/s12518-013-0120-x.

Ondiviela, B., Losada, I.J., Lara, J.L., Maza, M., Galván, C., Bouma, T.J., van Belzen, J., 2014. The role of seagrasses in coastal protection in a changing climate. Coast. Eng. 87, 158–168.

Paling, E.I., van Keulen, M., Wheeler, K., Phillips, J., Dyhrberg, R., 2001. Mechanical seagrass transplantation in Western Australia. Ecol. Eng. 16, 331–339.

Possingham, H.P., Bode, M., Klein, C.J., 2015. Optimal conservation outcomes require both restoration and protection. PLoS Biol. 13, e1002052.

Price, D.M., Robert, K., Callaway, A., Lo Iacono, C., Hall, R.A., Huvenne, V.A.I., 2019. Using 3D photogrammetry from ROV video to quantify cold-water coral reef structural complexity and investigate its influence on biodiversity and community assemblage. Coral Reefs 38, 1007–1021. https://doi.org/10.1007/s00338-019-01827-3.

Raoult, V., David, P.A., Dupont, S.F., Mathewson, C.P., O'Neill, S.J., Powell, N.N., Williamson, J.E., 2016. GoPros™ as an underwater photogrammetry tool for citizen science. PeerJ. 2016 Apr 25 4, e1960. https://doi.org/10.7717/peerj.1960. PMID: 27168973; PMCID: PMC4860335.

Rende, S.F., Irving, A.D., Bacci, T., Parlagreco, L., Bruno, F., De Filippo, F., Montefalcone, M., Penna, M., Trabucco, B., Di Mento, R., Cicero, A.M., 2015. Advances in micro-cartography: a two-dimensional photo mosaicing technique for seagrass monitoring. Estuar. Coast Shelf Sci. 167, 475–486. https://doi.org/10.1016/j.ecss.2015.10.029.

Rende, S.F., Bosman, A., Di Mento, R., Bruno, F., Lagudi, A., Irving, A.D., Dattola, L., Giambattista, L. Di, Lanera, P., Proietti, R., 2020. Ultra-high-resolution mapping of posidonia oceanica (L.) Delile meadows through acoustic, optical data and object-based image classification. J. Mar. Sci. Eng. 8, 647.

Rezek, R.J., Furman, B.T., Jung, R.P., Hall, M.O., Bell, S.S., 2019. Long-term performance of seagrass restoration projects in Florida, USA. Sci. Rep. 9, 1–11.

Sanz-Ablanedo, E., Chandler, J.H., Rodríguez-Pérez, J.R., Ordóñez, C., 2018. Accuracy of unmanned aerial vehicle (UAV) and SfM photogrammetry survey as a function of the number and location of ground control points used. Rem. Sens. 10, 1606.

Seytre, C., Francour, P., 2014. A long-term survey of Posidonia oceanica fish assemblages in a Mediterranean marine protected area: emphasis on stability and no-take area effectiveness. Mar. Freshw. Res. 65, 244–254.

Som-ard, J., Hossain, M.D., Ninsawat, S., Veerachitt, V., 2018. Pre-harvest sugarcane yield estimation using UAV-based RGB images and ground observation. Sugar Tech 20, 645–657.

Takasu, T., Yasuda, A., 2009. Development of the low-cost RTK-GPS receiver with an open source program package RTKLIB. In: Presentation at the International Symposium on GPS/GNSS, November 4–6, Seogwipo-Si Jungmun-Dong, Korea.

Telesca, L., Belluscio, A., Criscoli, A., Ardizzone, G., Apostolaki, E.T., Fraschetti, S., Gristina, M., Knittweis, L., Martin, C.S., Pergent, G., Alagna, A., Badalamenti, F., Garofalo, G., Gerakaris, V., Louise Pace, M., Pergent-Martini, C., Salomidi, M., 2015. Seagrass meadows (Posidonia oceanica) distribution and trajectories of change. Sci. Rep. 5, 1–14. https://doi.org/10.1038/srep12505.

Toniolo, C., Di Sotto, A., Di Giacomo, S., Ventura, D., Casoli, E., Belluscio, A., Nicoletti, M., Ardizzone, G., 2018. Seagrass Posidonia oceanica (L.) Delile as a marine biomarker: a metabolomic and toxicological analysis. Ecosphere 9. https://doi.org/10.1002/ecs2.2054.

Unsworth, R.K.F., McKenzie, L.J., Collier, C.J., Cullen-Unsworth, L.C., Duarte, C.M., Eklöf, J.S., Jarvis, J.C., Jones, B.L., Nordlund, L.M., 2019. Global challenges for seagrass conservation. Ambio 48, 801–815.

Van Katwijk, M.M., Bos, A.R., De Jonge, V.N., Hanssen, L., Hermus, D.C.R., De Jong, D.J., 2009. Guidelines for seagrass restoration: importance of habitat selection and donor population, spreading of risks, and ecosystem engineering effects. Mar. Pollut. Bull. 58, 179–188.

van Katwijk, M.M., Thorhaug, A., Marbà, N., Orth, R.J., Duarte, C.M., Kendrick, G.A., Althuizen, I.H.J., Balestri, E., Bernard, G., Cambridge, M.L., 2016. Global analysis of seagrass restoration: the importance of large-scale planting. J. Appl. Ecol. 53, 567–578.

Ventura, D., Dubois, S.F., Bonifazi, A., Jona Lasinio, G., Seminara, M., Gravina, M.F., Ardizzone, G., 2020. Integration of close-range underwater photogrammetry with inspection and mesh processing software: a novel approach for quantifying ecological dynamics of temperate biogenic reefs. Remote Sens. Ecol. Conserv. https://doi.org/10.1002/rse2.178.

Verduin, J.J., Paling, E.I., van Keulen, M., Rivers, L.E., 2012. Recovery of donor meadows of Posidonia sinuosa and Posidonia australis contributes to sustainable seagrass transplantation. Int. J. Ecol. 2012.

Walbridge, S., Slocum, N., Pobuda, M., Wright, D.J., 2018. Unified geomorphological analysis workflows with benthic terrain modeler. Geosci. 8 https://doi.org/10.3390/geosciences8030094.

Wan, L., Li, Y., Cen, H., Zhu, J., Yin, W., Wu, W., Zhu, H., Sun, D., Zhou, W., He, Y., 2018. Combining UAV-based vegetation indices and image classification to estimate flower number in oilseed rape. Remote Sens 10, 1484.

Wheaton, J.M., Brasington, J., Darby, S.E., Sear, D.A., 2010. Accounting for uncertainty in DEMs from repeat topographic surveys: improved sediment budgets. Earth Surf. Process. landforms J. Br. Geomorphol. Res. Gr. 35, 136–156.

Williams, J.G., Rosser, N.J., Hardy, R.J., Brain, M.J., Afana, A.A., 2018. Optimising 4D approaches to surface change detection: improving understanding of rockfall magnitude–frequency. Earth Surface Dynamics 6, 101–119.

Young, G.C., Dey, S., Rogers, A.D., Exton, D., 2017. Cost and time-effective method for multiscale measures of rugosity, fractal dimension, and vector dispersion from coral reef 3D models. PLoS One 12, 1–18. https://doi.org/10.1371/journal.pone.0175341.